ACS OMEGA

Article

http://pubs.acs.org/journal/acsodf

Structural Heterogeneity of CNGA1 Channels Revealed by Electrophysiology and Single-Molecule Force Spectroscopy

Sourav Maity,[†] Arin Marchesi,[‡] Vincent Torre,* and Monica Mazzolini*

International School for Advanced Studies (SISSA), Neuroscience Area, via Bonomea 265, 34136 Trieste, Italy

Supporting Information

ABSTRACT: The determination at atomic resolution of the three-dimensional molecular structure of membrane proteins such as receptors and several ion channels has been a major breakthrough in structural biology. The molecular structure of several members of the superfamily of voltage-gated ionic channels such as K^+ and Na^+ is now available. However, despite several attempts, the molecular structure at atomic resolution of the full cyclic nucleotide-gated (CNG) ion channel, although a member of the same superfamily of voltage-gated ion channels, has not been obtained yet, neither by X-ray crystallography nor by electron cryomicroscopy (cryo-EM). It is possible that CNG channels have a high structural heterogeneity, making difficult crystallization and single-particle analysis. To address this issue, we have combined single-molecule force spectroscopy (SMFS) and electrophysiological experiments to characterize the structural heterogeneity of CNGA1 channels expressed in *Xenopus laevis* oocytes. The unfolding of the cytoplasmic domain had force peaks, occurring with a probability from 0.2 to 0.96. Force peaks during the unfolding of the transmembrane domain had a probability close to 1, but the distribution of the increase in contour length between two successive force peaks had multiple maxima differing by tens of nanometers. Concomitant electrophysiological experiments showed that the rundown in mutant channels S399C is highly variable and that the effect of thiol reagents when specific residues were mutated was consistent with a dynamic structural heterogeneity. These results show that CNGA1 channels have a wide spectrum of native conformations that are difficult to detect with X-ray crystallography and cryo-EM.

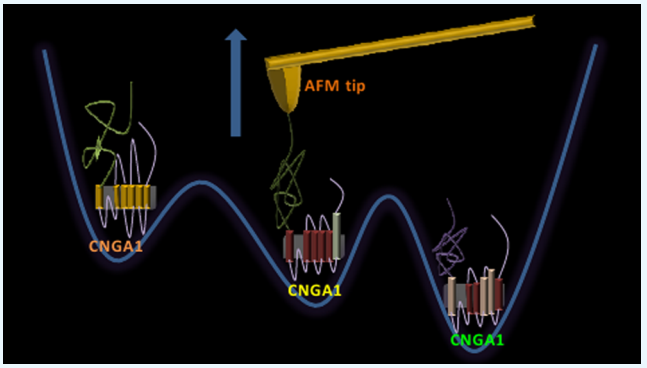

INTRODUCTION

The determination at atomic resolution of the three-dimensional (3D) molecular structure of several ion channels, such as voltage-gated ion channels like potassium and sodium channels,[1,2] has been a major breakthrough in structural biology. However, the structure of the full cyclic nucleotide-gated (CNG) ion channel, although a member of the same superfamily of voltage-gated ion channels, has not been obtained yet, neither by X-ray crystallography nor by electron cryomicroscopy (cryo-EM). CNG channels could have a large number of distinct conformational states[3] so that the usual methods for determining the 3D molecular structure fail. Indeed, crystallography captures only the most stable conformation among a variety of different states.[4,5] Crystallography and Cryo-EM require purified membrane proteins, which are subsequently analyzed in a nonphysiological environment (low temperature, detergent, and absence of the plasma membrane). Cryo-EM is a single-molecule technique and therefore can reveal, to some extent, the conformational transition and structural heterogeneity of an ionic channel, as demonstrated for TRPV1, TRPV2, and MloK1 channels.[6−10] Therefore, it is important to verify the degree of the structural heterogeneity of CNG channels, possibly in their native environment.

To address this issue, we have combined single-molecule force spectroscopy (SMFS) and electrophysiological experiments to characterize the structural heterogeneity of CNGA1 channels expressed in *Xenopus laevis* oocytes. SMFS provides some structural information at the single-molecule level under almost physiological conditions, useful to characterize the structural heterogeneity of membrane proteins. In SMFS experiments,[11−19] the protein under investigation is pulled and unfolded, and the resulting $F-D$ curve is composed of a series of force peaks. In these experiments, a drop of the force necessary to unfold the protein causes the appearance of a force peak: its occurrence signals that an unfolded region or a poorly structured polypeptide is in the process of being unfolded. If the protein to be unfolded is a membrane protein, such as an ion channel, then the unfolding of the transmembrane domain occurs sequentially so that it is possible to identify the location of the unfolded region with an accuracy of some amino acids

Received: August 22, 2016
Accepted: October 14, 2016
Published: December 13, 2016

DOI: 10.1021/acsomega.6b00202
ACS Omega 2016, 1, 1205−1219

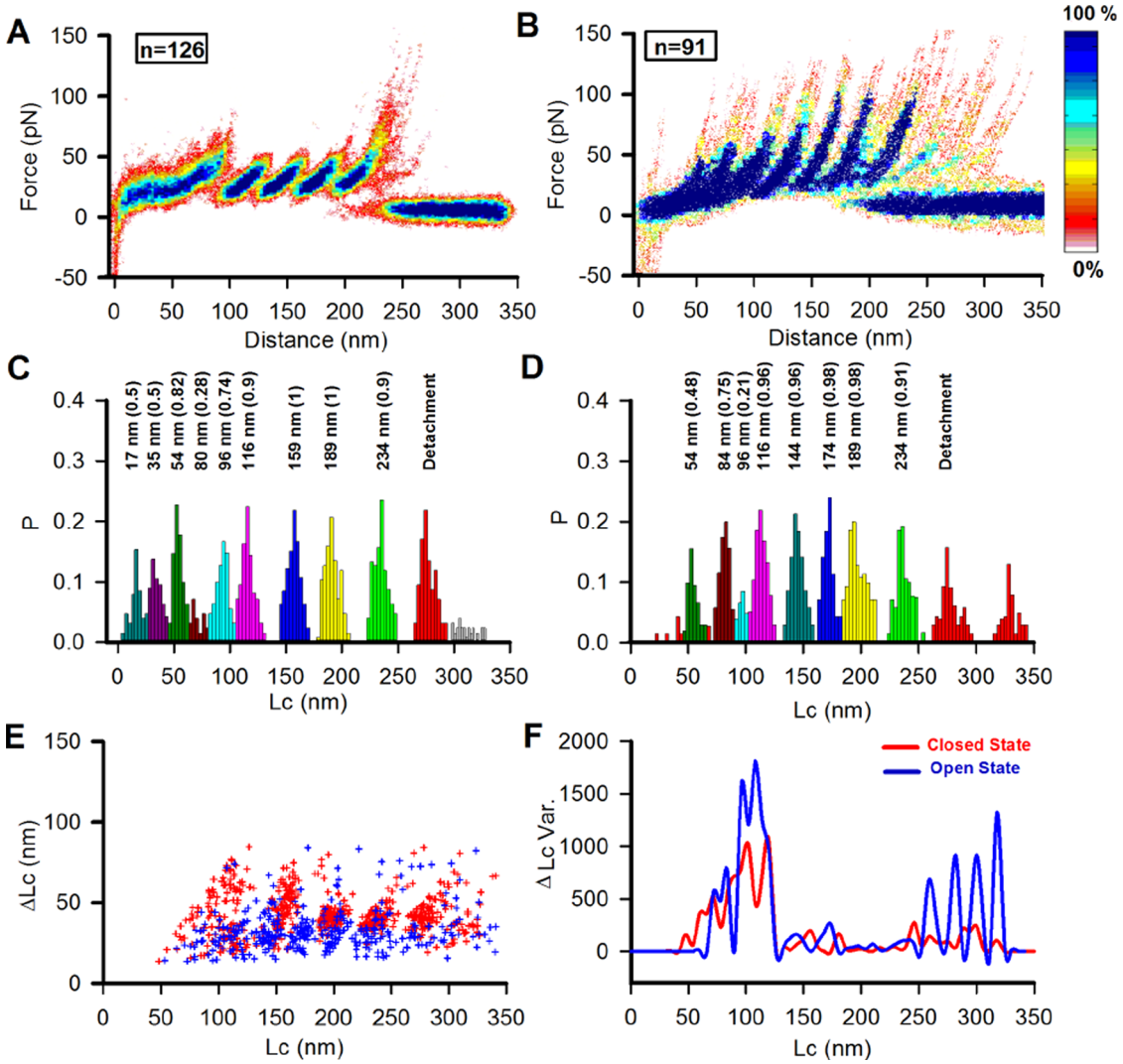

Figure 1. Unfolding variability of CNGA1 channels. (A, B) Density plots of *F*–*D* curves obtained from the unfolding of CNGA1 channels in the closed (126 curves) and open states (91 curves), respectively. (C) Histogram of the values of Lc obtained by fitting *F*–*D* curves with the WLC model in the closed state; force peaks with a value of Lc equal to 17 ± 2.4 (n = 63), 35 ± 3.6 (n = 63), 54 ± 2.8 (n = 104), 80 ± 4.8 (n = 36), 96 ± 3.6 (n = 94), and 116 ± 5.6 nm (n = 114) occurred with a probability of 0.50, 0.50, 0.82, 0.28, 0.74, and 0.90, respectively, and they are associated with the unfolding of the cytoplasmic domain. Force peaks with a value of Lc of 159 ± 5.6 (n = 126), 189 ± 6.4 (n = 126), and 234 ± 6.8 nm (n = 114) corresponding to the unfolding of the transmembrane domain occurred with a probability close to 1. (D) As in (C) but in the open state; force peaks with a value of Lc of 54 ± 3.2 (n = 44), 84 ± 4.0 (n = 69), 96 ± 2.4 (n = 19), and 116 ± 4.4 nm (n = 88) occurred with a probability of 0.48, 0.75, 0.31, and 0.96, respectively, and force peaks with a value of Lc of 144 ± 5.2 (n = 88), 174 ± 4.8 (n = 89), 189 ± 7.2 (n = 89), and 234 ± 5.6 nm (n = 83) occurred with a probability close to 1. In (C) and (D), the number above each peak indicates the value of Lc and its probability (P). Only forces larger above 35 pN were considered. (E) Mapping of *F*–*D* curves into the (Lc, ΔLc) plane in the closed (red points) and in the open states (blue points). In each *F*–*D* curve, the sequence of force peaks (F_1, F_2, ..., F_i, ..., F_n) and the corresponding sequence of the values of Lc (Lc_1, Lc_2, ..., Lc_i, ..., Lc_n) are identified; each *F*–*D* curve is mapped in the (Lc, ΔLc) plane into the set of n points (Lc_i, $\Delta Lc_i = Lc_i - Lc_{i-1}$) i = 1, ..., n. See Method for further details. (F) Comparison of the variance (var) of ΔLc for closed (in red) and open (in blue) states using a bin width of 5 nm.

(a.a.). The location of a force peak is obtained by fitting the experimental *F*–*D* curve with the Worm-Like Chain (WLC) model,[20,21] providing the values of the contour lengths (Lc). From the value of Lc, it is possible to estimate with a good accuracy the number of a.a.[21] as ΔLc/0.4 nm, where ΔLc is the increase of Lc between two consecutive force peaks of the unfolded polypeptide and therefore to probe the structural heterogeneity.[22,23] In a recent investigation,[24] we have used SMFS to examine conformational changes during the gating of CNGA1 channels that are expressed in *Xenopus laevis* oocytes,[25−27] that is, a physiological-like membrane and we observed the existence of multiple peaks in the distribution of the values of ΔLc between consecutive force peaks during the unfolding of the transmembrane domain of CNGA1 channels and in the present article, we extend this analysis to the cytoplasmic domain and to the N-terminal of these channels both in the open (in the presence of 2 mM cGMP) and closed states (in the absence of cGMP). We found a high variability, consistent with the existence of several distinct native conformations, confirmed by electrophysiological experiments.

RESULTS

Unfolding Variability of CNGA1 Channels in the Open and Closed States. Voltage-gated ion channels form a large superfamily including also CNG channels[25−31] that are opened by the binding of cyclic nucleotides with a gating, which is also

DOI: 10.1021/acsomega.6b00202
ACS Omega 2016, 1, 1205−1219

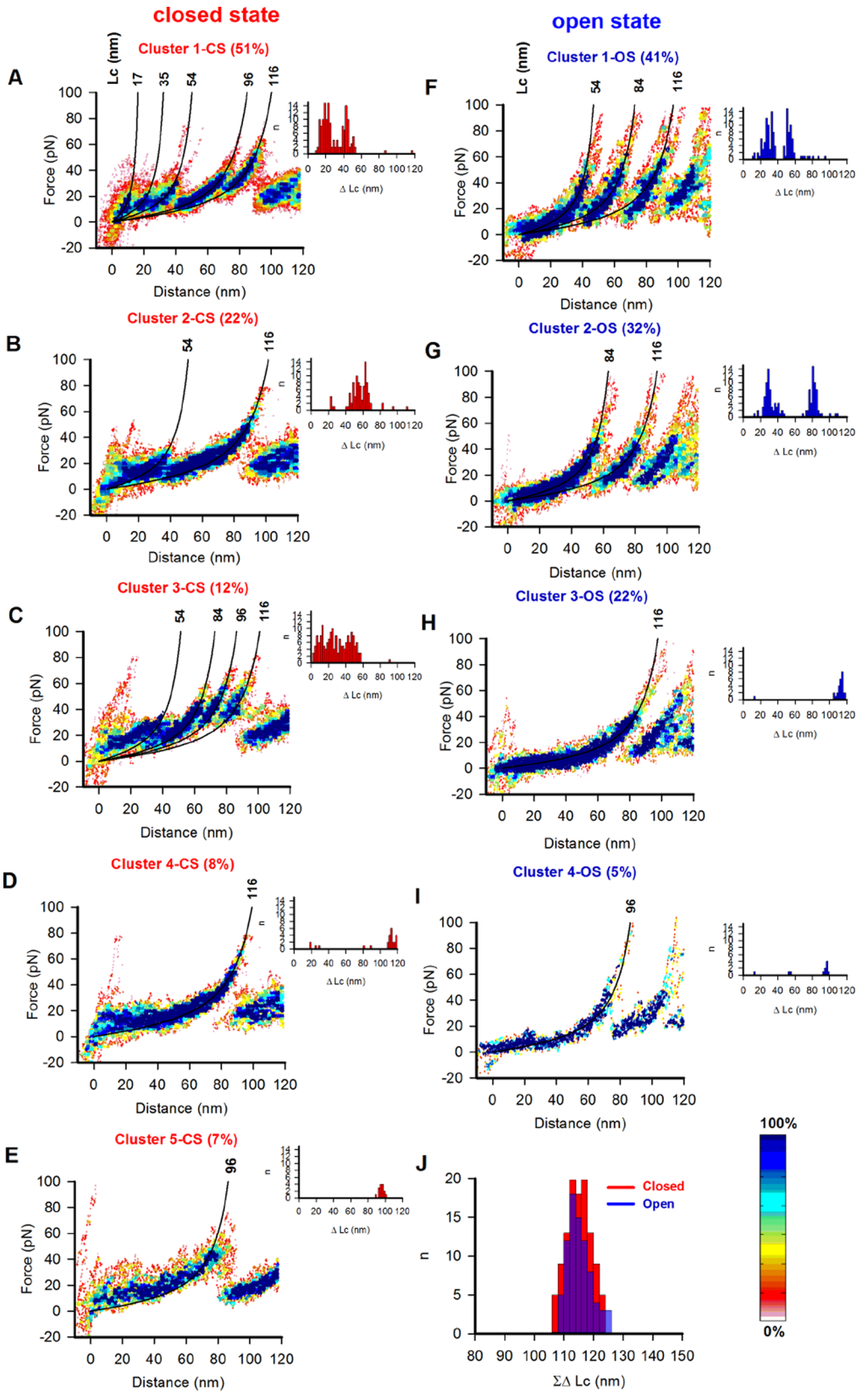

Figure 2. Variability of the unfolding of the cytoplasmic domain. (A) Density plot of *F*−*D* curves from CNGA1 channels in the closed state for cluster 1-CS (closed state here named CS) with an occurrence of 51% and force peaks with values of Lc of 17 ± 2.4, 35 ± 2.4, 54 ± 4.0, 96 ± 4.0, and 116 ± 3.2 nm (n = 64). (B) Density plot for cluster 2-CS with an occurrence of 22% and force peaks with values of Lc of 54 ± 4.0 and 116 ± 3.6 nm (n = 28). (C) Density plot for cluster 3-CS with an occurrence of 12% and force peaks with values of Lc of 54 ± 3.6, 84 ± 2.8, 96 ± 3.6, and 116 ± 4.0 nm (n = 15). (D) Density plot for cluster 4-CS with an occurrence of 8% and only a force peak with a value of Lc of 116 ± 3.6 nm (n = 11). (E) Density plot for cluster 5-CS with an occurrence of 7% and only a force peak with a value of Lc of 96 ± 3.2 nm (n = 9). The insets in panels (A)−(E) represent the histogram of the values of ΔLc for each *F*−*D* curve. (F) Density plot of *F*−*D* curves from CNGA1 channels in the open state

DOI: 10.1021/acsomega.6b00202
ACS Omega 2016, 1, 1205−1219

Figure 2. continued

for cluster 1-OS (open state here named OS), with an occurrence of 41% and force peaks with values of Lc of 54 ± 3.2, 84 ± 3.6, and 116 ± 4.8 nm (n = 38). (G) Density plot for cluster 2-OS with an occurrence of 32% and force peaks with values of Lc of 84 ± 3.2 and 116 ± 3.6 nm (n = 30). (H) Density plots for cluster 3-OS with an occurrence of 22% and only a force peak with a value of Lc of 116 ± 4.0 nm (n = 20). (I) Density plots for cluster 4-OS with an occurrence of 5% and only a force peak with a value of Lc of 96 ± 3.4 nm (n = 5). (J) Histogram of the sum of values of ΔLc of all of the $F-D$ curves up to 116 nm (i.e., unfolding of the cytoplasmic domain) in the open (blue) and closed (red) states. In all of the panels, solid black curves represent the fitting with the WLC model and the number indicates the corresponding value of Lc. In all of the density plots, the scale bar is as in Figure 1 and in all ΔLc, histogram bin = 2 nm. Here, we used procedure #1 for clustering as described in the Method section.

voltage-dependent.[25] CNG channels are formed by four subunits, either of type A (CNGA1, CNGA2, CNGA3, CNGA4, and CNGA5) or of type B (CNGB1 and CNGB2). CNGA1 channels are homomeric channels composed of four subunits and have functional properties similar, but not identical to, those of native CNG channels. The CNGA1 subunit from bovine rods is composed of 690 a.a., and hydropathicity and biochemical analyses[28] have identified six transmembrane α-helices referred as S1, S2, S3, S4, S5, and S6 that are linked by nonspanning loops, which are either extracellular or intracellular. There is a pore region between S5 and S6 where ion permeation occurs. Both the N- and C-terminals are cytoplasmic with the C-terminal (N400−D690) being a large domain composed of the C-linker (N400−E482) and the cyclic nucleotide binding (CNB) domain (A483−N610).[32,33] Although electrophysiological properties of these channels have been extensively clarified,[30,34,35] the full-length channel has never been crystallized. A low-resolution architecture obtained from single-particle imaging,[36] partial crystal structures of the CNB domain,[37−39] and the pore region of a mimic of CNGA1 channels[40,41] is available.

We have used SMFS and a bioinformatics analysis[24] to identify $F-D$ curves obtained from the unfolding of single CNGA1 subunits from their C-terminal expressed in *Xenopus laevis* oocytes. We identified 126 and 91 $F-D$ curves in the closed and in the open states, respectively. In these $F-D$ curves, the distance (D) coincides with the tip-sample separation[24] (TSS). The density plots (Figure 1A,1B, respectively) of these $F-D$ curves show five and seven main force peaks, above 50 pN, in the closed (Figure 1A) and open states (Figure 1B), respectively.

A closer inspection of $F-D$ curves allows the detection of additional force peaks not present in all $F-D$ curves and appearing with a force below 50 pN. In the closed state (Figure 1C), five force peaks with a value of Lc less than 100 nm were seen with forces between 35 and 50 pN. All of these force peaks have a probability (P) lower than 1. We identified four force peaks with a value of Lc higher than 100 nm and P close to 1 that appeared in almost all $F-D$ curves. These force peaks were followed by the detachment occurring with a value of Lc varying from 230 to 280 nm.

In the open state (Figure 1D), force peaks had larger amplitudes between 50 and 100 pN, and three force peaks with a value of Lc lower than 100 nm were detected with a value of P below 1. In the open state, five force peaks were present during the unfolding of the transmembrane domain and occurred with a value of P close to 1 (Figure 1B,D). The detachment, however, occurred with a larger variability than that observed in the closed state. To restrict our heterogeneity study to those $F-D$ curves, which were confirmed a complete unfolding of a single CNGA1 subunit (from its C-terminal), we have based our analysis on $F-D$ curves, which were obtained following the procedure, as described in our previous study.[24]

As the location of force peaks in $F-D$ curves is a key feature, we found it convenient to map each $F-D$ curve in a set of points in the (Lc, ΔLc) plane (see red and blue points for the closed and open states, respectively, in Figure 1E). This mapping allows visualizing the variability of the location of force peaks (Lc) and of the corresponding increase in Lc (ΔLc) from the previous force peak (see Method for further details). This mapping shows dispersed points for values of Lc below 116 nm and accumulation of points for values of Lc between 120 and 250 nm. Force peaks with values of Lc below 116 nm correspond to the unfolding of the cytoplasmic domain and those with values of Lc between 120 and 250 nm correspond to the unfolding of the transmembrane domain.[24] The accumulation of points in the (Lc, ΔLc) plane in restricted regions, for values of Lc between 120 and 250 nm, occurs because force peaks during the unfolding of the transmembrane domain have a value of P close to 1 (see Figure 1C,D). As a consequence, the variance of ΔLc (see red and blue traces in Figure 1F) is large for values of Lc below 116 nm and becomes low from 120 to 250 nm both in the closed and open states. In the open state, however, the variance of ΔLc is significantly higher beyond 250 nm.

In the density plots of Figure 1A,B, $F-D$ curves were aligned and individual $F-D$ curves were displaced by not more than 5 nm. This displacement, however, affects the exact determination of the value of Lc, but much less the value of ΔLc. Therefore, we focused the investigation of the unfolding variability on the force peaks with a value of P less than 1 and on the analysis of the distribution of the values of ΔLc.

Unfolding Variability of the Cytoplasmic Domain. As shown in Figure 1, force peaks with values of Lc below 116 nm occur with values of P lower than 1 and appear only in some $F-D$ curves (Figure 1C,D). Using the clustering procedure #1[24] (see also Method), we found several clusters of $F-D$ curves with a similar pattern during the unfolding of the cytoplasmic domain.

In the closed state, we found five major clusters (Figure 2A−E). The most frequent cluster 1-CS has four force peaks below 116 nm with an amplitude between 20 and 30 pN at 17 ± 2.4, 35 ± 2.4, and 54 ± 4.0 nm (n = 64) and with an amplitude around 40 ± 15 pN at 96 ± 4.0 nm (n = 64). Clusters 2-CS and 3-CS have a lower number of force peaks (Figure 2B,C) with values of Lc below 116 nm. Cluster 4-CS has a single force peak with a value of Lc of 116 ± 4.0 nm (Figure 2D, n = 11), whereas cluster 5-CS has a single force peak with a value of Lc of 96 ± 3.2 nm (Figure 2E, n = 9). In the open state, we found four major clusters with a lower number of force peaks and different values of P (Figure 2F−I): force peaks with values of Lc below 50 nm were not observed, in contrast with what often seen in the closed state (see Figure 2A). In cluster 1-OS, there are three force peaks with an Lc equal to 54 ± 3.2, 84 ± 3.6, and 116 ± 4.8 nm (n = 38). Cluster 2-OS has two force peaks with an Lc of 84 ± 3.2 and 116 ± 3.6 nm (n = 30), whereas

DOI: 10.1021/acsomega.6b00202
ACS Omega 2016, 1, 1205−1219

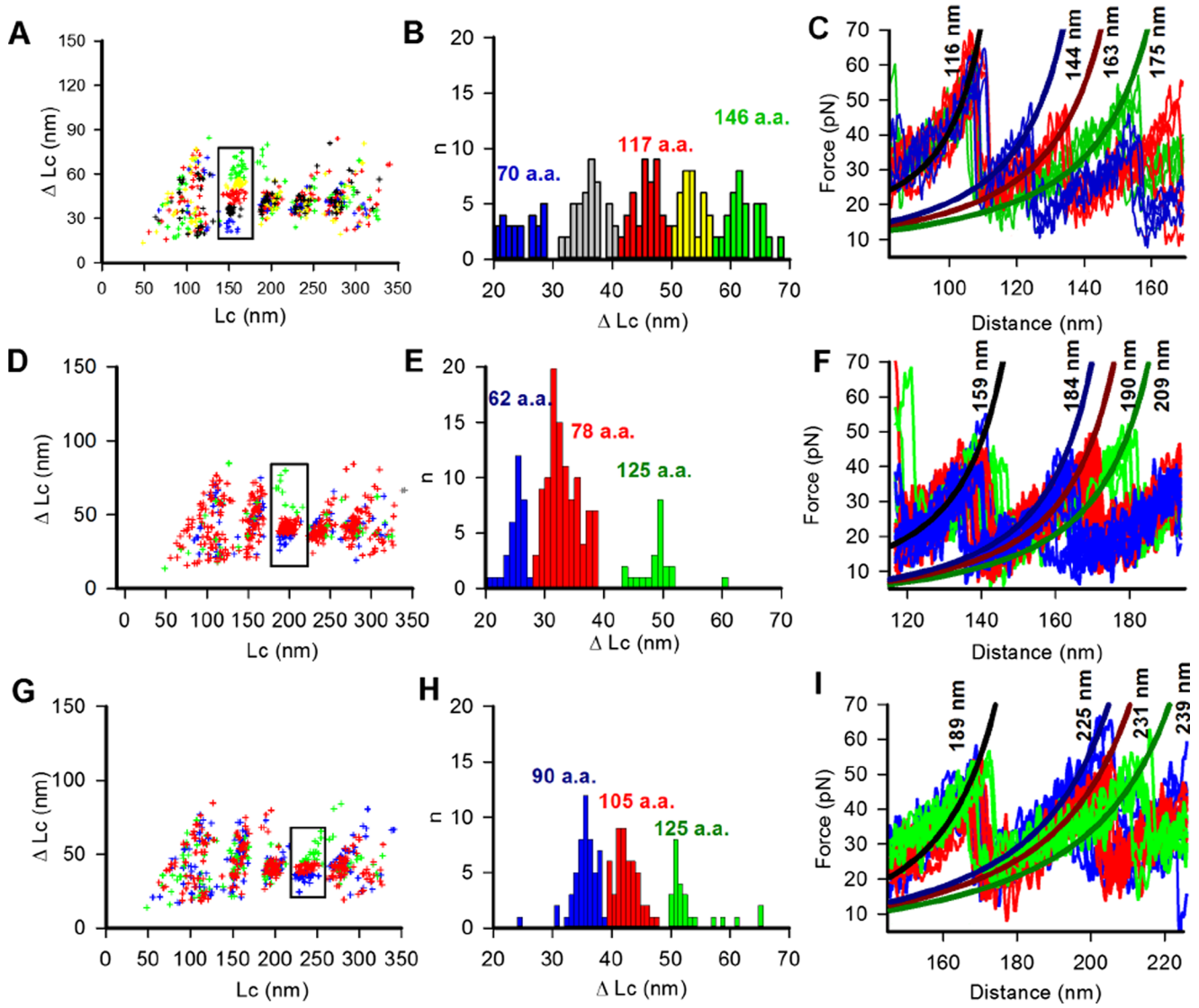

Figure 3. Variability of ΔLc for the transmembrane domain in the closed state. (A) Mapping of *F*−*D* curves into the (Lc, ΔLc) plane in the closed state where values of ΔLc associated with Lc around 159 nm, within the rectangular box, were analyzed. (B) Histogram of the values of ΔLc in the rectangular box of panel a. The histogram has five peaks that were identified with a different color, which was also used to identify the corresponding points within the rectangular box of a. As each *F*−*D* curve corresponds to a set of distinct values in the (Lc, ΔLc) plane, the color used within the rectangular box to label an *F*−*D* curve with a given value of ΔLc is used to for all points corresponding to that *F*−*D* curve. (C) Examples of *F*−*D* curves corresponding to the blue, green, and red points in b aligned so as to have a coincident force peak with an Lc of 116 nm. (D) and (E) as in (A) and (B), but for values of ΔLc associated with Lc around 189 nm. (F) as in (C) but *F*−*D* curves aligned to a common force peak with an Lc of 159 nm. (G) and (H) as in (A) and (B), but for values of ΔLc associated with Lc around 234 nm. (I) as in (C) but *F*−*D* curves aligned to a common force peak with an Lc of 189 nm. In (A), (D), and (G), procedure #2 for clustering is used (see Method and also Figure S1).

clusters 3-OS and 4-OS have only one force peak with an Lc of 116 ± 4.0 nm (n = 20) and 96 ± 3.4 nm (n = 5), respectively.

The histograms of the values of ΔLc for clusters 1−4 in the closed state and for clusters 1−3 in the open state have multiple peaks (see insets in the corresponding panels), but the sum of ΔLc ($\sum$ΔLc) has a Gaussian distribution with only one peak both for the closed and open states (Figure 2J). This behavior is similar to that observed during the unfolding of the T4 lisozyme and the leucine binding protein,[22,23] for which the sum of ΔLc has a Gaussian distribution with only one peak. The unfolding of *F*−*D* curves belonging to clusters 5-CS and 4-OS follows a different mechanism, in which a large portion of the cytoplasmic domain is unfolded in a single step but another portion of it unfolds concomitantly to the unfolding of the transmembrane domain.

Unfolding Variability of the Transmembrane Domain.

Both in the closed and open states, the force peaks with an Lc between 116 and 234 nm, corresponding to the unfolding of the transmembrane domain, have a probability between 0.9 and 1 (Figure 1). In the closed state, points in the (Lc, ΔLc) plane accumulate around values of Lc of 159, 189, and 234 nm, and we analyzed in detail the points in the rectangular boxes (see Figure 3A,D,G). The histogram of the values of Lc of points in these boxes had Gaussian distribution in agreement with what is seen in Figure 1C. Rather unexpectedly, however, the histogram of the values of ΔLc corresponding to the increase in Lc between two successive force peaks was not Gaussian-distributed but had multiple peaks: in the closed state, the histogram of ΔLc between the force peaks at about 116 and 159 nm (Figure 3B) had five peaks and the histograms of ΔLc

DOI: 10.1021/acsomega.6b00202
ACS Omega 2016, 1, 1205−1219

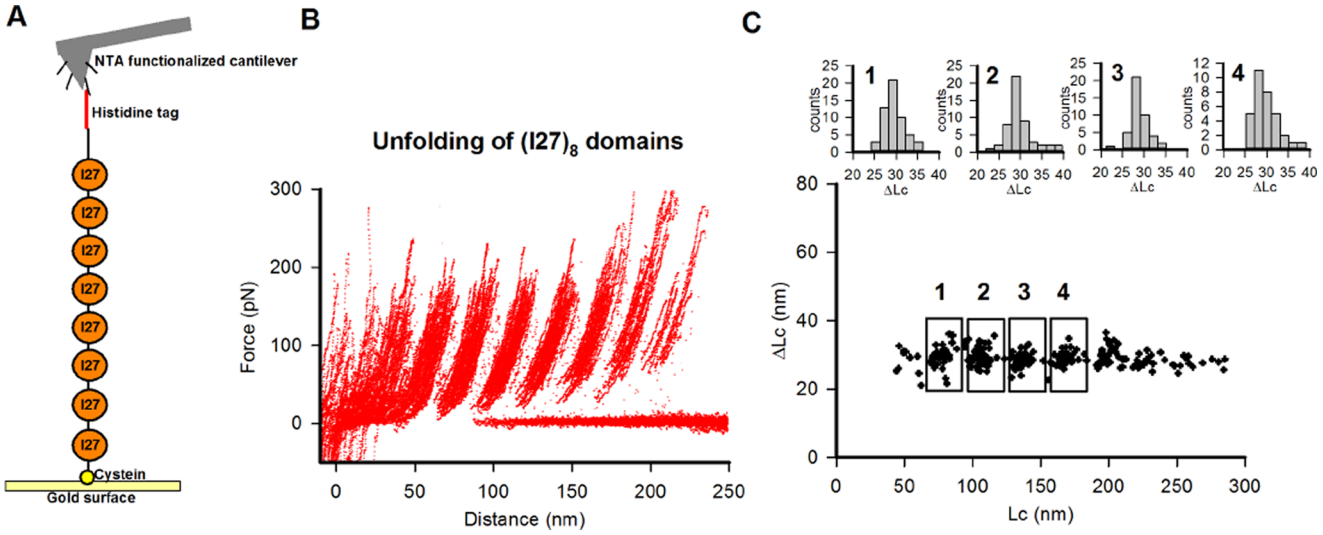

Figure 4. Unfolding of polypeptide chain composed of eight modules of I27; (A) Schematic of the polypeptide chain composed of eight modules of I27. The chain contains cysteine in one side to bind covalently to the gold surface, and on the other side fused with six histidine tag to bind specifically to the gold-coated atomic force microscopy (AFM) cantilever, functionalized with NTA−Ni^{2+}. (B) Family of *F*−*D* traces obtained from the unfolding of the I27 chains shown in (A); (C) The distributions of the values of ΔLc from the points in the (Lc, ΔLc) plane, shown in the lower portion, within the four solid boxes.

between the force peaks at about 159 and 189 nm (Figure 3E) and at about 189 and 234 nm (Figure 3H) had three peaks. Using procedure #2 (see Method and Figure S1), points in the (Lc, ΔLc) plane were clustered (see colors in Figure 3A,D,G) according to the peaks found in the histogram of ΔLc values. When *F*−*D* curves were aligned so as to have a common force peak at 159 nm (Figure 3C), 189 nm (Figure 3F), and 234 nm (Figure 3K), the successive force peaks appeared at distinct values of ΔLc in agreement with what is seen in Figure 3B,E,H. Similar results were obtained also for the open state (see Figure S2).

Peaks of ΔLc varied from approximately 25 to 65 nm and assuming that the length of a single a.a. is 0.4, the number of a.a. unfolded between two successive force peaks varied from about 60 to 150. This large variability indicates a high structural heterogeneity of the transmembrane α-helices S1, S2, S3, S4, S5, and S6, which are significantly larger than that suggested by the molecular structure of voltage-gated ionic channels, such as K^+ and Na^+ channels, obtained from crystallization and X-ray diffraction.[1,2] To verify whether the presence of multiple peaks in the distribution of the values of ΔLc was caused by some artifacts in our recoding system and not by a genuine structural heterogeneity of CNGA1 channels, we performed SMFS experiments on a chain of polypeptides formed by eight repetitions of the I27 modules, anchored to a gold surface by an cysteine positioned at the start of the polypeptide (Figure 4A). The chain is fused with six histidine tag (His-tag) to bind specifically to a gold-coated tip, functionalized with nitrilotriacetic acid (NTA)−Ni^{2+}, which provides sufficient anchoring force to unfold a structurally stable I27 module with a mechanical stability of force of ∼180 pN.[21] The I27 module is properly folded, and no significant structural heterogeneity is expected.[21] From these experiments, we obtained 58 *F*−*D* curves (Figure 4B) with force peaks with an amplitude of about 180 pN with a mean ΔLc value of approximately 28 nm, a well-known signature of the unfolding of the I27 module. From these *F*−*D* curves, we obtained the values of (Lc, ΔLc) in the corresponding plane (lower portion of Figure 4C), and we computed the distribution of the values of ΔLc within the four boxes shown in the (Lc, ΔLc) plane. As shown in Figure 4C (upper portion), the histograms of the values of ΔLc have a single peak, different from that shown in Figure 3. These control experiments were performed in the same manner as during the unfolding of CNGA1 channels.

Electrophysiological Validation of the Structural Variability. After the overexpression of CNGA1 channels in the plasma membrane of *Xenopus laevis* oocytes and using the excised patch technique and electrical measurements, it is possible to analyze the properties of wild-type and mutant channels where specific amino acids are mutated, one by one, in cysteine. These experiments provide in most cases highly reproducible results but for some mutant channels, we observed a significant variability, which indicates the existence of structural heterogeneity. We have analyzed electrophysiological experiments performed in our laboratory in the last 2 decades in search of an independent validation of the structural heterogeneity suggested by SMFS experiments. We have performed several cysteine scanning mutagenesis (CSM) in different regions of CNGA1 channels. In CSM experiments, a residue is mutated into a cysteine and the effect of sulfhydryl reagents, such as Cd^{2+}, copper phenantroline (CuP), and 2-(trimethylammonium)ethyl methanethiosulfonate bromide (MTSET), is analyzed. Cd^{2+} ions usually coordinate to two sulfur (S) atoms,[42,43] and CuP[44,45] promotes the formation of disulfide bonds, and their effects are mediated and therefore reveal the closeness of two S atoms.[46,47] MTSET binds to a single S atom, and its effect reveals the accessibility of mutated residues.[46,47]

In the cytoplasmic domain, we performed a CSM from D588 to N610. In the closed state, Cd^{2+} and CuP blocked the great majority of these cysteine mutants, whereas MTSET blocked only some of the mutant channels[33] (Figure S3). In the open state, a similar diffuse blockage was not observed. These results strongly indicate that channel blockage occurs when one exogenous S atom from one subunit of these mutant channels enters in close proximity (less than 14 Å) to the homologous S

DOI: 10.1021/acsomega.6b00202
ACS Omega 2016, 1, 1205−1219

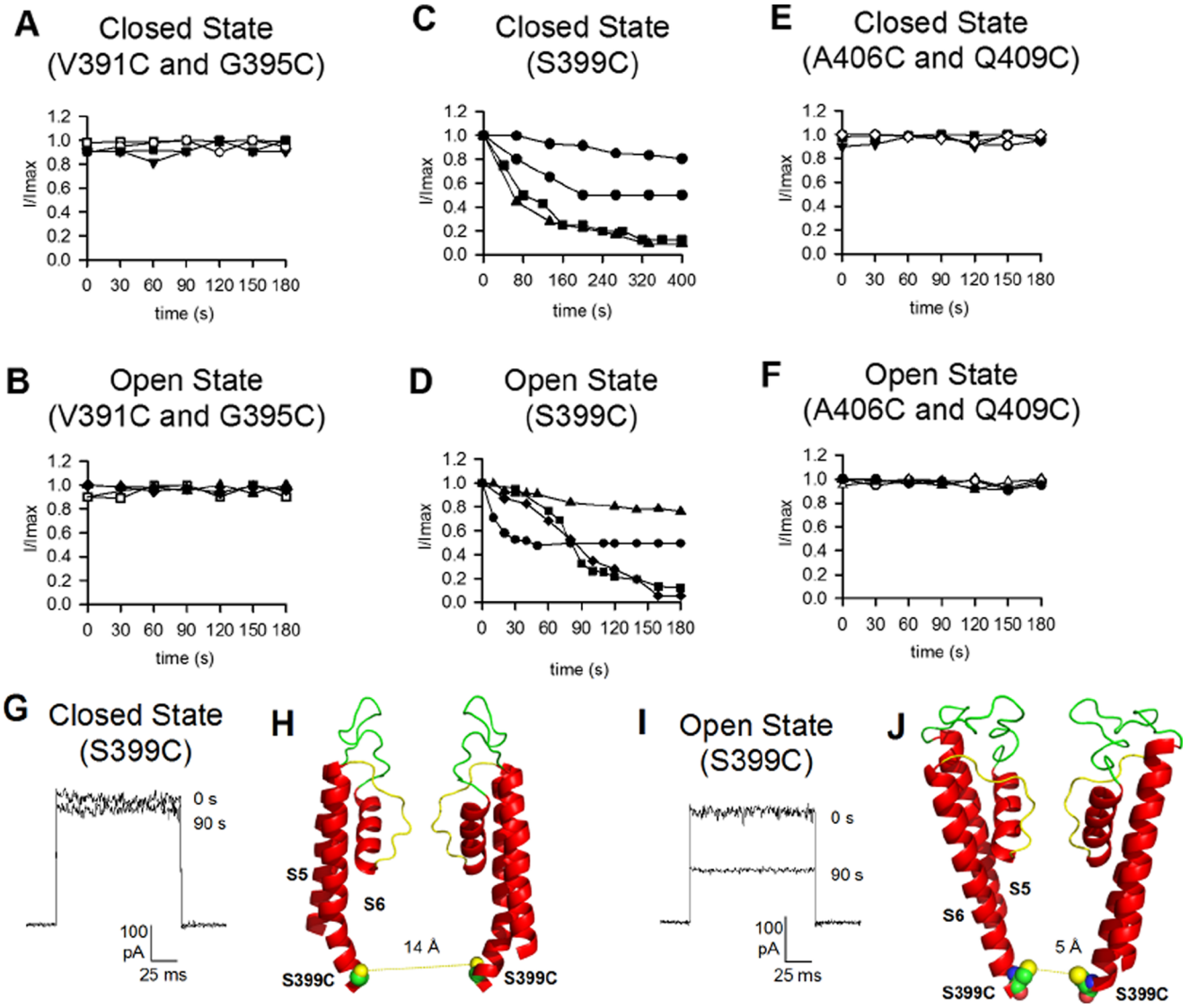

Figure 5. Variability of the unfolding of the S6 transmembrane domain. (A) Normalized amplitude of current recordings at +60 mV against time for the mutant channels V391C (white symbol $n = 2$) and G395C (black symbol $n = 2$) measured in an inside-out excised patch under voltage-clamp conditions in the closed state. Time 0 corresponds approximately, with a delay of 20−40 s, to the time when the patch was excised from the oocyte. Currents were normalized to the value measured at time 0. (B) The same as in (A) but in the open state ($n = 2$ and 2, respectively). (C) As in (A) but for the mutant channel S399C ($n = 4$) in the closed state. (D) As in (C) but in the open state ($n = 4$). (E, F) As in (A) and (B) but for the mutant channels A406C (white symbol) and Q409C (black symbol) in the closed (E) and open (F) states. (G) Current recordings at +60 mV in the presence of 2 mM cGMP at the beginning of the experiment and after 90 s. Almost no rundown was observed; (H) schematic of the S5 and S6 transmembrane domains based on the molecular structure of the Kv1.2−Kv2.1 channel in which residues in position 399 are far away and do not form an S−S bond so that no rundown is observed; (I) As in (G) but in this case a significant rundown was observed within 90 s; (J) Schematic of the S5 and S6 transmembrane domains inspired by the molecular structure of the K channel in which residues in position 399 are near and could form an S−S bond so that rundown is observed.

atom of another subunit or an endogenous S atom, possibly belonging to C481 or C505 or C573. As originally proposed,[33] these electrophysiological experiments indicate that in the closed state, residues from D588 to L607 are parts of highly mobile chains of a.a. so that exogenous cysteines become in close proximity to either other exogenous or endogenous cysteines and provide an independent and complementary validation of the structural heterogeneity suggested by SMFS data (Figure 2). In the open state, in contrast, a similar diffuse blockage is not observed[33] (Figure S3), suggesting a lower structural heterogeneity in the presence of cGMP, in agreement with the disappearance of force peaks with values of Lc lower than 50 nm (see Figure 2F−H).

Measurements of the single-channel conductance of the blocking effect of divalent cations (such as Ca^{2+} and Mg^{2+}) and of the effect of temperature have always provided highly reproducible results but in CSM experiments when some specific residues were mutated into a cysteine, we observed a consistent variability in the outcome of electrophysiological experiments.

The highest variability in the plot of (Lc, ΔLc) is observed at TSS around 100 nm, corresponding to the interface between the cytoplasmic domain and the intracellular side of S6 (Figures 1F and 3) and therefore we performed a CSM in this region. If mutated residues of neighboring subunits are close, then disulfide bonds will form and the closure of the channel is

DOI: 10.1021/acsomega.6b00202
ACS Omega 2016, 1, 1205−1219

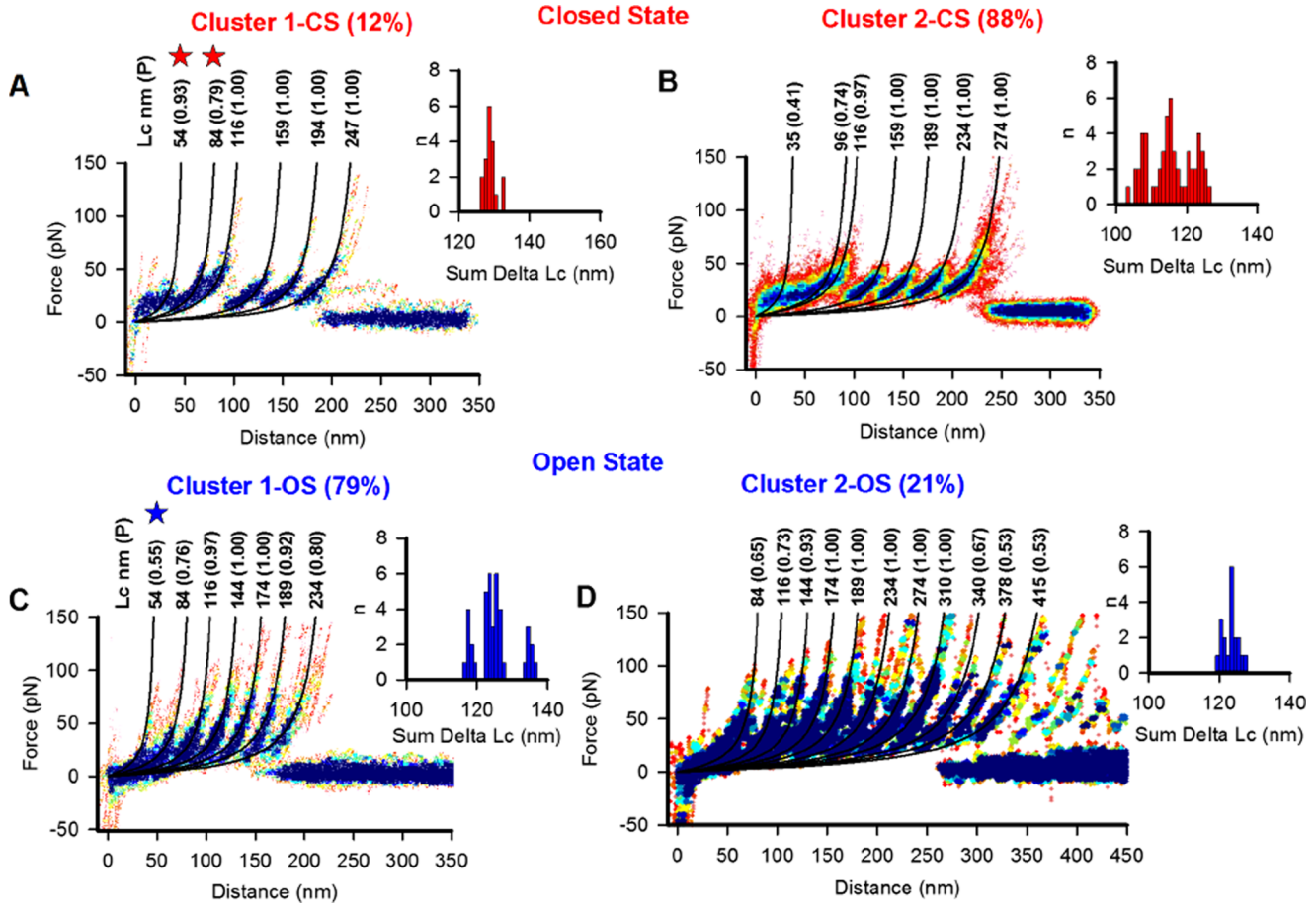

Figure 6. Variability of detachment. (A, B) Density plots of *F*−*D* curves from the unfolding CNGA1 channels in the closed state ending with a force peak with a value of Lc around 247 ± 5.6 (n = 15) and 274 ± 7.2 nm (n = 111), respectively (point 1 unit). *F*−*D* curves in (A) have the detachment coinciding with the unfolding of the last transmembrane segment S1, whereas for those in (B), detachment occurs with an extra peak. *F*−*D* curves in (A) have initial force peaks with a value of Lc of 54 ± 2.0 (n = 14) and 84 ± 2.4 nm (n = 12) (see red stars), not present in *F*−*D* curves in (B). Clusters in (A) and (B) occurred with an occurrence of 12 and 88%. (C, D) Density plots of *F*−*D* curves from the unfolding CNGA1 channels in the open state ending with a force peak with a value of Lc of 234 ± 2.8 nm (n = 72) and larger than 300 nm, respectively (point size 1 unit in (E) and 1.5 unit in (G)). *F*−*D* curves in (C) have the detachment coinciding with the unfolding of the last transmembrane segment S1, whereas for those in (D), detachment occurs with a large value of Lc. Almost 50% of *F*−*D* curves in (C) have a force peak with a value of Lc of 54 ± 3.2 nm (n = 40, see blue star), not present in *F*−*D* curves in (D). Clusters in (C) and (D) occurred with an occurrence of 79 and 21%, respectively. The insets in panels (A)−(D) represent the sum of the values of ΔLc for each *F*−*D* curve. In all density plots, the scale bar is as in Figure 1.

expected: under these circumstances, a rundown of the cGMP-activated current will be observed also in the absence of sulfhydryl reagents. Therefore, we looked to the occurrence of the rundown of the cGMP-activated current in membrane patches from mutant channels V391C, G395C, and S399C (Figure 5). Mutant channels V391C and G395C consistently and in all experiments did not exhibit any rundown (Figure 5A,B) over a period between 5 and 15 min. In mutant channel S399C, in contrast, both in the closed (Figure 5C) and open (Figure 5D) states, highly variable results were observed. In some experiments, an almost complete rundown was observed within 180 s, revealing the closeness of the exogenous cysteines, whereas in other experiments, very little rundown was observed because the exogenous cysteines could not form disulfide bonds. Similar to that observed with mutant channels V391C and G395C, we did not observe any rundown either in mutant channel A406C or Q409C (Figure 5E,F). We performed a CSM also in the pore region from R345C to S371C, and we did not observe any rundown in these mutant channels with the exception of the mutant channel I361C. In this mutant channel, the rundown was complete within 60 s and was highly reproducible,[48] indicating that in this mutant channel the exogenous cysteines are invariably at a close distance.

Inspection of the available molecular structures of members of the family of voltage-gated ion channels offers a possible explanation for the variable rundown of mutant channel S399C: in the chimera Kv2.1−Kv1.2,[32,51,52] the S6 domain bends toward outside the pore axis and becomes connected to the C-linker and if the CNGA1 channel adopts a similar conformation, then residues S399 in neighboring subunits are at a distance larger than 14 Å and no disulfide bonds can be formed in mutant channel S399C (Figure 5G,H). In contrast, if the S6 α-helix adopts an orientation reminiscent of closed K channels,[49,50] then residues S399 can become in proximity so that in mutant channel S399C disulfide bonds are formed (Figure 5J).[51]

Over the years, we mutated into a cysteine more than 130 residues of CNGA1 channels and in almost all mutant channels the effect of MTSET was highly reproducible.[33,48,51−53] However, we observed some variability when residues near the cytoplasmic end of S4 were mutated into cysteines. In some patches, exposure to MTSET in the closed state did not

DOI: 10.1021/acsomega.6b00202
ACS Omega 2016, 1, 1205−1219

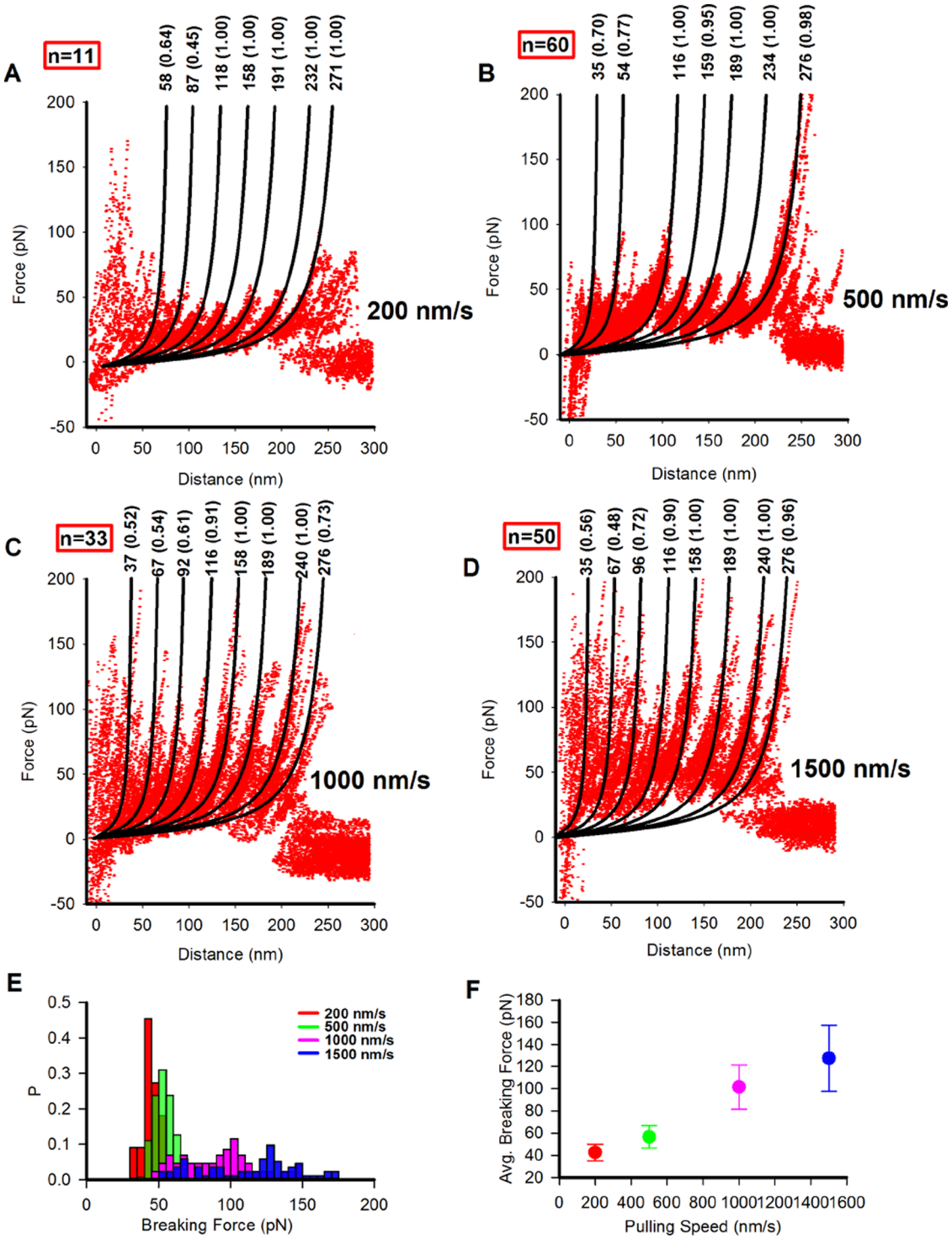

Figure 7. Pulling speed dependency of CNGA1 unfolding. (A–D) Superposition of *F–D* curves from CNGA1 channels unfolding with a pulling speed of 200, 500, 1000, and 1500 nm/s, respectively; the black lines represent the WLC fitting with indicated value of Lc. The *P* values are reported in bracket above the value of Lc. (E) Comparison of the breaking force distribution, that is, corresponding to the detachment, for each pulling speed. The red, green, pink, and blue colors represent the pulling speed of 200, 500, 1000, and 1500 nm/s, respectively. (F) The plot of average peak force vs pulling speed. The number of superimposed *F–D* curves in (A)–(D) was 11, 60, 33, and 50 for the pulling speed of 200, 500, 1000, and 1500 nm/s collected from the same batches of injected oocytes.

produce any detectable change in cGMP-activated current both in mutant channels T290C and F282C (see Figure S4), whereas in other patches, MTSET produced a detectable potentiation at negative voltages and a concomitant reduction of the voltage rectification seen before exposure to MTSET. A similar variability was observed when MTSET was added in the open state. These results suggest that the exogenous cysteines in positions 282 and 290 have a variable accessibility from the intracellular side, supporting the notion of the existence of different native conformations of CNGA1 channels. We propose that when MTSET is attached to these exogenous cysteines, fluctuations of the motion of the voltage sensor S4

DOI: 10.1021/acsomega.6b00202
ACS Omega 2016, 1, 1205–1219

are reduced, leading to a reduction of the mild voltage rectification observed under control conditions.

The results of these electrophysiological experiments (Figures S3 and S4) provide a confirmation that the variability observed in SMFS experiments is caused by a significant structural heterogeneity of CNGA1 channels and that different configurations could vary in some cases up to 10 Å and even more (Figure 5C,F).

Variability of Detachment. In the closed state, approximately 12% of the *F*−*D* curves show detachment corresponding to a value of Lc equal to 247 ± 5.6 nm (Figure 6A, $n = 15$). Both the C- and N-terminals of CNGA1 channels are intracellular so that when the C-terminal is pulled the detachment is expected to occur at the beginning of S1 because there is no anchoring force at the N-terminal. However, the remaining 88% *F*−*D* curves show an additional force peak at around 274 ± 7.2 nm (Figure 6B, $n = 111$), which corresponds approximately to the full length of the channel (690 a.a.), suggesting that the N-terminal is not free but it is anchored to some other structure. Short and longer *F*−*D* curves are very similar, but not entirely: indeed, short traces have clear force peaks with a value of Lc about 54 ± 2.0 ($n = 14$) and 84 ± 2.4 nm ($n = 12$) with P equal to 0.93 and 0.79, respectively, whereas longer *F*−*D* curves do not have force peaks around 54 and 84 nm but were displaced at 35 ± 6.9 nm ($n = 46$, $P = 0.41$) and 96 ± 3.5 nm ($n = 82$, $P = 0.74$).

In the open state, some of the *F*−*D* curves had final detachment, with a value of Lc about 234 ± 2.8 nm (Figure 6C, $n = 72$), similar to that observed in the closed state and with $P = 0.79$, but other *F*−*D* curves were significantly longer (Figure 6D). In these *F*−*D* curves, force peaks appeared replicated, as obtained from the unfolding of not a single CNGA1 subunit, but from the concatenation of two subunits. Indeed, in the open state, the N-terminal of one subunit strongly interacts with the C-terminal of a neighboring subunit[54,55] so that two neighboring subunits are almost linked together: under these conditions, when the cantilever tip unfolds one CNGA1 subunit, an additional subunit can subsequently be unfolded. In the open state, shorter *F*−*D* curves have a force peak with Lc around 54 ± 3.2 nm ($n = 13$) with $P = 0.55$. This force is not observed in longer *F*−*D* curves, suggesting that, similar to that observed in the closed state, when the unfolding of the CNGA1 channel requires a force peak with a value of Lc around 54 ± 3.2 nm ($n = 13$), its C-terminal is less prone to interaction with the N-terminal of a neighboring subunit. This possibility is also supported by the observation that *F*−*D* curves obtained from the CNGA1−CNGA1 tandem construct do not show force peaks with values of Lc around 54 nm.[24] Therefore, our results indicate a possible moderate interaction between the N- and C-terminals in the closed state, potentiated in the open state where the N-terminal can either be free or interacting with neighboring subunits.

We have also computed the sum of ΔLc corresponding to the unfolding of the transmembrane domain ($\sum_{TM}\Delta Lc$) corresponding to portions of the *F*−*D* curves between the force peak at about 116 nm and that at about 234 nm,[24] and we analyzed its variability. For short *F*−*D* curves (Figure 6A), in the closed state, the value of $\sum_{TM}\Delta Lc$ has only one peak with a value of about 130 nm with a Gaussian distribution (inset Figure 6A), whereas for longer *F*−*D* curves (Figure 6B), the distribution of $\sum_{TM}\Delta Lc$ had three peaks at 108, 115, and 128 nm (inset Figure 6B). The number of force peaks in the distribution of $\sum_{TM}\Delta Lc$ is linked to the presence of specific force peaks during the unfolding of the cytoplasmic domain. Indeed, in the closed state, if during the unfolding of the cytoplasmic domain there are force peaks with a value of Lc at 54 ± 2.0 and 84 ± 2.4 nm ($n = 72$), then detachment occurs at about 247 nm, suggesting that in this case the C-terminal of CNGA1 channels is almost free. In contrast, if detachment occurs at about 274 nm, then the value of $\sum_{TM}\Delta Lc$ has multiple peaks. We have also computed $\sum_{TM}\Delta Lc$ for *F*−*D* curves obtained in the open state in contrast to that seen in the closed state; shorter *F*−*D* curves had three peaks at 118, 125, and 134 nm (compare insets of Figure 6A,C), whereas longer *F*−*D* curves had only one peak at 128 nm (inset Figure 6D).

We have also observed a significant coupling between the unfolding of the cytoplasmic and transmembrane domains especially in the closed state (see Figure S5) and at a lower extent in the open state (see Figure S6)

Unfolding at Different Speeds. When the pulling speed is 500 nm/s, the cytoplasmic domain unfolds with a variable number of force peaks, whereas the transmembrane domain unfolds with an almost fixed number of force peaks but with highly different values of ΔLc. It is possible, however, that this unfolding pattern was caused by the used pulling speed and does not represent a distinct feature of the unfolding of CNGA1 subunit and a signature of its structural heterogeneity. Therefore, we compared *F*−*D* curves obtained from the unfolding of CNGA1 subunits at pulling speeds from 200 to 1500 nm/s. As expected from previous investigations,[13,56] a large force was necessary to unfold CNGA1 when the pulling speed was increased (Figure 7) but the value of Lc corresponding to the observed force peaks did not change their mean value. At a slower pulling speed of 200 nm/s, the force necessary to unfold CNGA1 channels was often lower than 50 pN (Figure 7A), and the force peaks observed during the unfolding of the TM domain had a probability larger than 0.9, but a higher variability was observed during the unfolding of the cytoplasmic domain. Similar results were obtained at the pulling speed of 1000 nm/s (Figure 7C) and 1500 nm/s (Figure 7D). The unfolding force of a protein depends on the pulling speed of the cantilever.[57,58] According to the Bell−Evans model, the force of unfolding is proportional to the logarithm of the pulling speed. Because of our experimental limitations, we are only able to change the pulling velocity at a smaller scale, which is why the unfolding force scaled almost linearly with the pulling speed (Figure 7E,F).

DISCUSSION

The unfolding of CNGA1 channels expressed in *Xenopus laevis* oocytes is highly variable both in the number of force peaks (Figures 1 and 2) and in the values of ΔLc between successive force peaks (Figure 3) and follows a specific pattern. This variability is usually attributed to the existence of multiple native configurations and/or to its intrinsic stochasticity.[22,23] However, electrophysiological experiments with mutant channels, in which a specific a.a. is mutated in a cysteine and the spontaneous rundown is observed (Figure 5), combined with additional electrophysiological results (see Figures S3 and S4), suggest the existence of multiple native configurations of CNGA1 channels both in the closed and open states. The unfolding of the cytoplasmic domain occurs with a variable number of force peaks (Figure 2), up to three in the open state (Figure 2F−I) and up to four in the closed state (Figure 2A−E). The existence of more intermediate steps during the unfolding of the cytoplasmic domain in the closed state is likely

DOI: 10.1021/acsomega.6b00202
ACS Omega 2016, 1, 1205−1219

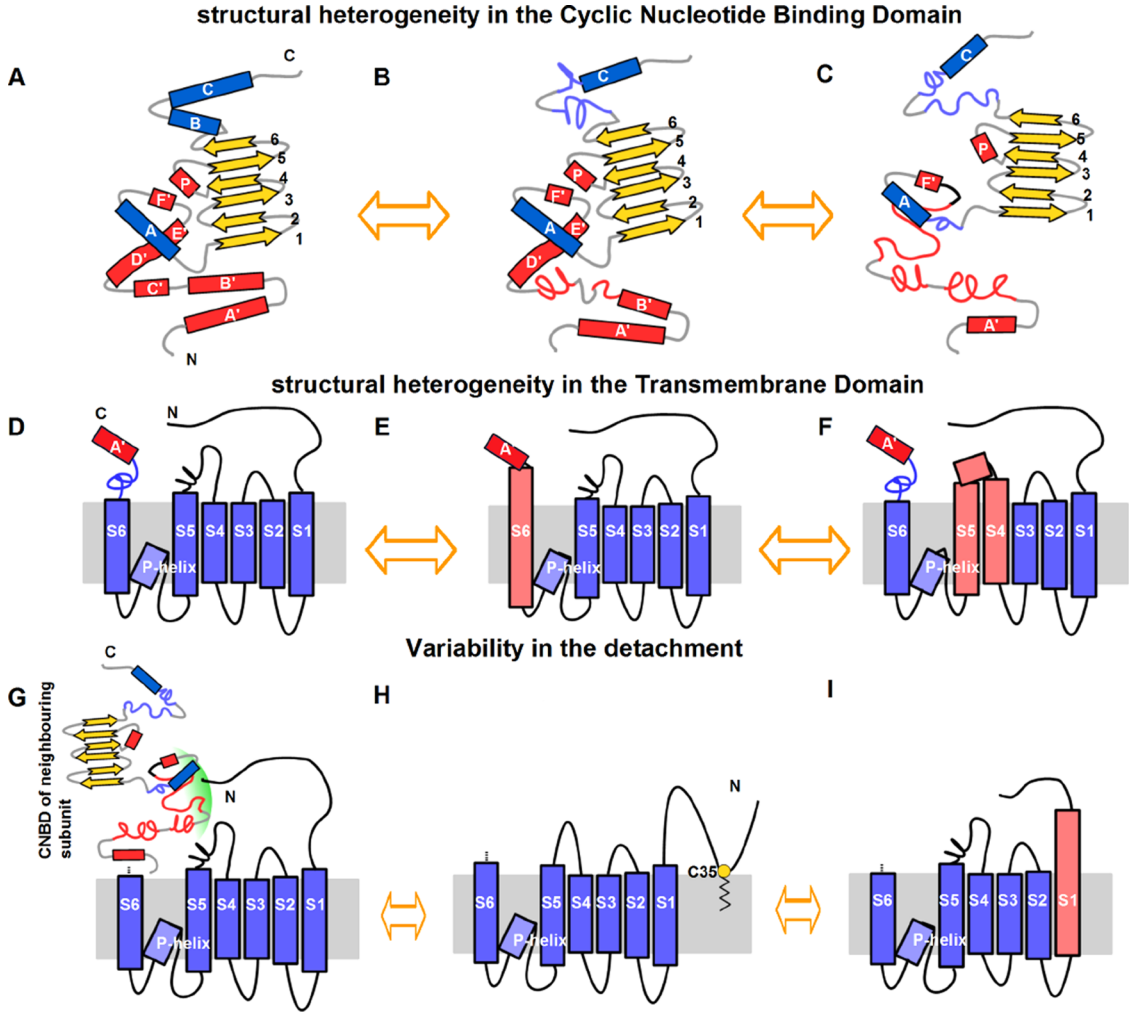

Figure 8. Schematic representation of the structural heterogeneity of CNGA1; (A–C) structural heterogeneity of CNB domain; three possible conformations: with all α-helices properly folded (A), a couple of α-helices partially unfolded (B), and many α-helices unfolded (C). (D–F) structural heterogeneity of transmembrane domain; three possible conformations: with the C-terminal end of S6 and the S4–S5 linker unfolded (D), with S6 properly folded and with a tight mechanical connection to the C-linker (E) with a highly rigid S5–S4 linker (F); (G–I) structural heterogeneity of the N-terminal. Three possible conformations: the N-terminal interacts with the CNB domain of a neighboring subunit (G), the N-terminal interacts with a membrane (H), and the N-terminal is free with S1 properly folded (I).

to be caused by a larger number of different conformations with the α-helices of the cyclic nucleotide binding domain (CNBD) properly folded, partially folded, or completely unfolded, as exemplified in Figure 8A–C. In the open state, the CNBD is likely to be more folded and to have a lower number of intermediate conformations in agreement with the AFM imaging of the cytoplasmic domain of the MlotiK1 potassium channels, which have a well-defined tetrameric structure only in the presence of cyclic nucleotides.[7] In a different way, the unfolding of the transmembrane domain occurs with an almost fixed number of force peaks but with highly variable values of ΔLc (Figures 1 and 3) both in the closed and open states. Indeed, the number of a.a. unfolded between two successive force peaks varies from some tens up to 120. This observation suggests that the α-helices forming the transmembrane domain preserve their topology of crossing the lipid membrane from the intracellular to the extracellular side but do not have a fixed configuration. In this view, the number of properly folded α-helix turns is variable, and the extracellular and intracellular loops connecting the α-helices have variable breaking points when stretched, as illustrated in Figure 8D–F where the number of properly folded turns of the transmembrane α-helices varies from 6 to 9.

The folding of α-helices is due to weak H-bonds and favorable side-chain interactions so that it is very sensitive to fluctuations in the local environment and to its degree of crowding and hydrophobicity.[59]

Also, the detachment following the unfolding of CNGA1 channels is highly variable (Figure 6), which can be rationalized by assuming that the N-terminal is a mobile and dynamic structure, and that in the open state a strong interaction with a neighboring subunit leads to the unfolding of two concatenated CNGA1 subunits (Figure 6G). The possible structural heterogeneity of the N-terminal is illustrated in the schematic of Figure 8G–J.

The existence of multiple conformations of ion channels is also supported by a detailed analysis of single-channel activity in which multiple open and closed states are necessary to explain the distribution of closed and open times.[3] The same conclusion can be drawn from molecular dynamic simulations of the glutamate receptors,[60] of Na^+ channels,[61] and of K^+ channels.[62] The existence of multiple conformational states

DOI: 10.1021/acsomega.6b00202
ACS Omega 2016, 1, 1205–1219

seems to be an emerging common property in most membrane proteins, such as the β2-adrenergic receptor.[4,5] Multiple conformations can originate not only from small movements of single a.a. but also from large movements of entire domains.[4,5] Simple thermal fluctuations, fluctuations in the oxidizing/reducing local environment, and the presence of conformations corresponding to local minima of the free-energy landscape all contribute to the structural variability.

Therefore, the obvious question is: how large are the structural differences of these conformations and how is it possible to measure them in a reliable way? The high variability of the spontaneous rundown of mutant S399C (Figure 5) suggests that structural differences of native conformations could be up to 10 Å and even larger.

The structural heterogeneity of CNGA1 channels, described here, is at the basis of the results of electrophysiological experiments in which residues in the CNBD were mutated, one by one, to a cysteine and the effect of thiol reagents was analyzed: as already proposed some years ago,[33] residues from D588 to L607 in the closed state, but not in the open state, are not part of a properly folded α-helix but belong to a highly mobile chain of polypeptides that assumes multiple conformations. As discussed in the main text, the structural heterogeneity of CNGA1 channels is also at the origin of the variability of the results of some electrophysiological experiments (Figures 5, S3, and S4).

CNGA1 channels and all other CNG channels are poorly selective and indeed are permeable to all monovalent alkali cations such as Li^+, Na^+, K^+, Rb^+, and Cs^+.[25,63] On the basis of physical considerations from statistical mechanics and thermodynamics,[64] this poor ionic selectivity was attributed to the flexibility of the pore of CNG channels, that is, to the capacity of the pore to adopt different configurations depending on which ion is present inside the pore. This hypothesis was later confirmed by X-ray crystallography,[41] in which the structure of the pore walls changed with the radius of the ion present inside the pore. The flexibility of the pore, as a consequence of the structural heterogeneity of CNGA1 channels, is also responsible for the voltage-dependent gating observed in the presence of large permeant cations, such as Cs^+ and dymethylamonium, but not with the small alkali cations such as Li^+, Na^+, and K^+.[25] In this case, when a large permeant cation is present in the pore, the pore walls expand so that it becomes sensitive to the motion of the voltage sensor located in S4.

Our results suggest to consider with caution the fixed and frozen folding of α-helices of membrane proteins obtained from X-ray crystallography, which could be produced by the combination of purification and the molecular forces caused by the strong packing inside diffracting crystals. When an ion channel is embedded in a natural membrane at room temperature, the static folding of its α-helices seen in X-ray crystallography is expected to become dynamic: the high variability of the values of ΔLc in the transmembrane domain (Figure 3) suggests that turns of transmembrane α-helices are formed and disrupted almost continuously.

CNGA1 channels, despite many attempts and efforts, have never been crystallized, and a possible explanation for their resistance to form well-ordered crystals able to diffract X-rays is their structural heterogeneity.

METHODS

Heterologous Expression System and Sample Preparation. RNA coding for the CNGA1 subunit was injected into *Xenopus laevis* oocytes ("Xenopus express" Ancienne Ecole de Vernassal, Le Bourg 43270, Vernassal, Haute Loire, France). Oocytes were prepared as previously described.[33] Injected oocytes were maintained at 18 °C in a Barth solution supplemented with 50 mg/mL of gentamycin sulfate and contained (in mM) 88 NaCl, 1 KCl, 0.82 $MgSO_4$, 0.33 $Ca(NO_3)_2$, 0.41 $CaCl_2$, 2.4 $NaHCO_3$, and 5 Tris−HCl (pH 7.4 buffered with NaOH). All of the used salts and reagents were purchased from Sigma-Aldrich (St. Louis, MO). The vitelline membrane of oocytes was removed mechanically. We performed SMFS in oocytes in which the cGMP-activated current measured with conventional patch pipettes was larger than 1 nA at ±100 mV.[24] These oocytes were incubated and deposited on a freshly cleaved mica substrate for 5−10 min in the recording solution (110 mM NaCl, 10 mM *N*-(2-hydroxyethyl)piperazine-*N*′-ethanesulfonic acid, 0.1 mM ethylenediaminetetraacetic acid, pH 7.4). After this step, we roll out the oocyte from the substrate leaving the attached piece of membrane on the substrate. The yolk and granules of the cytoplasm were removed by repetitive washings with the recording solution. To image the membrane patches, AFM in liquid and in tapping mode was used.

AFM and Cantilever Functionalization. In this study, we have used the AFM (NanoWizard 3, JPK) mounted upon an inverted optical microscope (Olympus IX71). After localizing plasma membrane patches, we performed SMFS experiments.[24] The cantilever spring constant was ∼0.08 N/m and was calibrated before the start of each experiment by using the equipartition theorem. A 0.4 NA/10× objective was used to localize the area of oocyte incubation. AFM images were acquired with a resolution of 512 pixels. For SMFS experiments, the tip was in contact with the selected membrane patch for 0.5 s while we applied a force of 1 nN. The surface was separated at a velocity of 500 nm/s while the force exerted between the tip and surface was recorded. During an experimental session lasting up to 8−10 h, approximately 10 000 *F*−*D* curves were collected in three or four different regions of 1 μm^2 size. We have performed similar SMFS experiments also when the pulling speed[13,56] was varied from 200 to 1500 nm/s.

Cantilever tips were functionalized with thiol and NTA−Ni^{2+}. The functionalization was done in four steps. First, tips were cleaned in ethanol for 15 min, dried under N_2 flow and exposed to ultraviolet light for 15 min. The tips were further incubated for 15 min in chloroform and dried again under a N_2 flow. These three steps were then repeated to obtain cleaner tips. In the second step, the cleaned cantilevers were incubated for 30 min in 10 μM dithiobis-C_2-NTA (Dojindo Molecular Technologies, Inc., Japan), washed with ethanol, and dried in a N_2 flow. In the third step, the tips were then incubated for 20 min in 100 μM $NiSO_4$ and rinsed with MilliQ water before being dried in a N_2 flow. Finally, the functionalized tips were incubated for 20 min in 10 mM 6-mercapto-1-hexanol to avoid nonspecific adsorption and were dried under a N_2 flow. Salts and reagents were purchased from Sigma-Aldrich.

SMFS Experiments and Data Processing. Clean fragments of oocyte membrane remained anchored to the mica substrate with the intracellular side exposed to the recording solution and to the cantilever tip of the AFM were used. After the localization of the membrane patch, we moved the AFM tip over the imaged area expressing CNGA1 channels. The CNGA1 concentration on the oocyte membrane depends on the level of expression of the CNGA1 channel. In electro-

DOI: 10.1021/acsomega.6b00202
ACS Omega 2016, 1, 1205−1219

physiological experiments with patch electrodes with a tip of about 1 μm^2, 24 h after injection of the mRNA into oocytes, it is possible to have electrical recordings from a single CNGA1 channel and in this case we have a very low channel density. After 3−5 days, it is possible to record currents in the nanoampere range and the number of CNGA1 channels can be 1000−5000 per μm^2.[24] Moreover, it is known that there are only few native membrane proteins present in oocytes[24,27] and only very few and almost none ionic channels of the family of voltage-gated channels. These are the conditions in which we performed our SMFS experiments. In approximately 20% of cases, the tip was able to absorb a molecule providing a sawtooth-like *F*−*D* curve and if the magnitude of force of these *F*−*D* curves was larger than 45 pN, the curve was saved. We performed SMFS and collected approximately 300 000 *F*−*D* curves in the absence of 2 mM cGMP (closed state) and 200 000 *F*−*D* curves in the presence of 2 mM cGMP (open state) from noninjected (control) oocytes. We also collected more than 500 000 *F*−*D* curves from oocytes that had been injected with the mRNA of CNGA1 channels in the open and closed states. We applied informatics to identify *F*−*D* curves that were present in only the SMFS experiments that used injected oocytes. The method had two steps. First, each *F*−*D* curve was mapped in a sequence of symbols that represented the location and amplitude of the force peaks (coding) and then these sequences were assembled in groups with similar properties (clustering). This method has been described in detail previously.[24]

Clustering of *F*−*D* Curves. To obtain and characterize the unfolding variability, we used two procedures for clusterization of *F*−*D* curves. Procedure #1 was similar to that already developed[24] and was used to identify the clusters of *F*−*D* curves associated with the unfolding of the C domain (see Figure 3). In this case, we restricted the analysis to values of TSS less than 120 nm and we identified four and three clusters for the closed and open states, respectively. In addition to procedure #1, we developed an additional procedure, referred as clustering procedure #2, for clustering of *F*−*D* curves on the basis of the mapping of each *F*−*D* curve in a set of points in the (Lc, ΔLc) plane shown in Figure S1. The clustering procedure #2 is composed of the following steps:

1 After the identification of *F*−*D* curves obtained from the unfolding of a single CNGA1 subunit,[24] each *F*−*D* curve is mapped in the (Lc, ΔLc) plane in the following way: each force peak F_i (larger than 35 pN) in a *F*−*D* curve is fitted with the WLC model[20,21] to obtain the corresponding value of Lc. In this way, the sequence of force peaks (F_1, F_2, ..., F_i, ...,F_n) is identified in the corresponding sequence of the values of Lc (Lc_1, Lc_2, ..., Lc_i, ..., Lc_n) and each *F*−*D* curve is mapped in the (Lc, ΔLc) plane into a set of n points (Lc_i, $\Delta Lc_i = Lc_i - Lc_{i-1}$) $i = 1, ..., n$.
2 Points in the (Lc, ΔLc) plane appear to accumulate in specific restricted regions as within the rectangular box of Figure S1B. Clustering is based on the analysis of the histogram of the values of ΔLc within these regions. As shown in Figure 1C, the histogram of the values of ΔLc is not Gaussian-distributed but has three distinct peaks, leading to three clusters indicated by different colors.
3 From the three clusters seen in Figure 1C, three sets of *F*−*D* curves are obtained and are mapped in the (Lc, ΔLc) plane as points with the same color (see Figure S1b). From these points, we can recover the corresponding *F*−*D* curves, as shown in Figures S5 and S6.

Ethics Statements. All experiments performed with *Xenopus laevis* frogs in this study were approved by the International School for Advanced Studies Ethics Committee according to the Italian and European guidelines for animal care (d.l. 116/92; 86/609/C.E.). Oocytes were harvested from female *Xenopus laevis* frogs using an aseptic technique or, if necessary, purchased from Ecocyte Bioscience (Am Förderturm, 44575, Castrop-Rauxel, Germany). All *X. laevis* surgeries were performed under general anesthesia, induced by immersion in a 0.2% solution of tricaine methane sulfonate (MS-222) adjusted to pH 7.4 for 15−20 min. Depth of anesthesia was assessed by loss of the righting reflex and loss of withdrawal reflex to a toe pinch. After surgery, animals were singly housed for 48 h. Frogs were monitored daily for 1 week postoperatively to ensure the absence of any surgery-related stress.

■ ASSOCIATED CONTENT

Supporting Information

The Supporting Information is available free of charge on the ACS Publications website at DOI: 10.1021/acsomega.6b00202.

Clusterization method based on the analysis of points in the (Lc, ΔLc) plane; variability of ΔLc for the transmembrane domain in the open state; effect of sulfhydryl reagents in the CNB domain; variability in the electrophysiological response of the S4 transmembrane domain; coupling between the unfolding of the cytoplasmic and transmembrane domains in the closed state; variability of the unfolding of the cytoplasmic and transmembrane domains in the open state (PDF)

■ AUTHOR INFORMATION

Corresponding Authors

*E-mail: torre@sissa.it (V.T.).
*E-mail: mazzolin@sissa.it (M.M.).

Present Addresses

†(S.M.) Moleculaire Biofysica, Zernike Instituut, Rijksuniversiteit Groningen, Nijenborgh 4, 9747 AG Groningen, The Netherlands.
‡(A.M.) INSERM U1006, Parc Scientifique et Technologique de Luminy, Bâtiment Inserm TPR2 bloc 5, Post Box 909, 163 avenue de Luminy, 13009 Marseille, France.

Author Contributions

S.M. performed SMFS experiments and data analysis; M.M. performed mutagenesis; M.M. and A.M. performed electrophysiology; S.M. and V.T performed bioinformatics; M.M. and V.T. performed data analysis of electrophysiology experiments; S.M., M.M., and V.T. designed the experiments; S.M., M.M., and V.T. participated in interpreting results; S.M., M.M., and V.T. contributed to writing of the article; and M.M and V.T. supervised the project.

Notes

The authors declare no competing financial interest.

■ ACKNOWLEDGMENTS

We thank F. Romagnoli for checking the English. This work was supported by FOCUS Contract no. 270483 (FP7-ICT-2009-6) from the EU.

DOI: 10.1021/acsomega.6b00202
ACS Omega 2016, 1, 1205−1219

REFERENCES

(1) Long, S. B.; Campbell, E. B.; Mackinnon, R. Crystal structure of a mammalian voltage-dependent Shaker family K+ channel. *Science* **2005**, *309*, 897−903.

(2) Payandeh, J.; Scheuer, T.; Zheng, N.; Catterall, W. A. The crystal structure of a voltage-gated sodium channel. *Nature* **2011**, *475*, 353−358.

(3) Brams, M.; Kusch, J.; Spurny, R.; Benndorf, K.; Ulens, C. Family of prokaryote cyclic nucleotide-modulated ion channels. *Proc. Natl. Acad. Sci. U.S.A.* **2014**, *111*, 7855−7860.

(4) Nygaard, R.; Zou, Y.; Dror, R. O.; Mildorf, T. J.; Arlow, D. H.; Manglik, A.; Pan, A. C.; Liu, C. W.; Fung, J. J.; Bokoch, M. P.; Thian, F. S.; Kobilka, T. S.; Shaw, D. E.; Mueller, L.; Prosser, R. S.; Kobilka, B. K. The dynamic process of β(2)-adrenergic receptor activation. *Cell* **2013**, *152*, 532−542.

(5) Manglik, A.; Kim, T. H.; Masureel, M.; Altenbach, C.; Yang, Z.; Hilger, D.; Lerch, M. T.; Kobilka, T. S.; Thian, F. S.; Hubbell, W. L.; Prosser, R. S.; Kobilka, B. K. Structural Insights into the Dynamic Process of β2-Adrenergic Receptor Signaling. *Cell* **2015**, *161*, 1101−1011.

(6) Liao, M.; Cao, E.; Julius, D.; Cheng, Y. Structure of the TRPV1 ion channel determined by electron cryo-microscopy. *Nature* **2013**, *504*, 107−112.

(7) Kowal, J.; Chami, M.; Baumgartner, P.; Arheit, M.; Chiu, P. L.; Rangl, M.; Scheuring, S.; Schröder, G. F.; Nimigean, C. M.; Stahlberg, H. Ligand-induced structural changes in the cyclic nucleotide-modulated potassium channel MloK1. *Nat. Commun.* **2014**, *5*, No. 3106.

(8) Vinothkumar, K. R. Membrane protein structures without crystals, by single particle electron cryomicroscopy. *Curr. Opin. Struct. Biol.* **2015**, *33*, 103−114.

(9) Huynh, K. W.; Cohen, M. R.; Jiang, J.; Samanta, A.; Lodowski, D. T.; Zhou, Z. H.; Moiseenkova-Bell, V. Y. Structure of the full-length TRPV2 channel by cryo-EM. *Nat. Commun.* **2016**, *7*, No. 11130.

(10) Zubcevic, L.; Herzik, M. A., Jr.; Chung, B. C.; Liu, Z.; Lander, G. C.; Lee, S. Y. Cryo-electron microscopy structure of the TRPV2 ion channel. *Nat. Struct. Mol. Biol.* **2016**, *23*, 180−186.

(11) Oesterhelt, F.; Oesterhelt, D.; Pfeiffer, M.; Engel, A.; Gaub, H. E.; Müller, D. J. Unfolding pathways of individual bacteriorhodopsins. *Science* **2000**, *288*, 143−146.

(12) Tanuj Sapra, K.; Park, P. S.; Filipek, S.; Engel, A.; Müller, D. J.; Palczewski, K. Detecting molecular interactions that stabilize native bovine rhodopsin. *J. Mol. Biol.* **2006**, *358*, 255−269.

(13) Kawamura, S.; Gerstung, M.; Colozo, A. T.; Helenius, J.; Maeda, A.; Beerenwinkel, N.; Park, P. S.; Müller, D. J. Kinetic, energetic, and mechanical differences between dark-state rhodopsin and opsin. *Structure* **2013**, *21*, 426−437.

(14) Kedrov, A.; Ziegler, C.; Muller, D. J. Differentiating ligand and inhibitor interactions of a single antiporter. *J. Mol. Biol.* **2006**, *362*, 925−932.

(15) Ge, L.; Perez, C.; Waclawska, I.; Ziegler, C.; Muller, D. J. Locating an extracellular K+-dependent interaction site that modulates betaine-binding of the Na+-coupled betaine symporter BetP. *Proc. Natl. Acad. Sci. U.S.A.* **2011**, *108*, E890−E898.

(16) Bosshart, P. D.; Iordanov, I.; Garzon-Coral, C.; Demange, P.; Engel, A.; Milon, A.; Müller, D. J. The TM protein KpOmpA anchoring the outer membrane of *Klebsiella pneumoniae* unfolds and refolds in response to tensile load. *Structure* **2012**, *20*, 121−127.

(17) Zocher, M.; Zhang, C.; Rasmussen, S. G.; Kobilka, B. K.; Müller, D. J. Cholesterol increases kinetic, energetic, and mechanical stability of the human β2-adrenergic receptor. *Proc. Natl. Acad. Sci. U.S.A.* **2012**, *109*, E3463−E3472.

(18) Jan, L. Y.; Jan, Y. N. A superfamily of ion channels. *Nature* **1990**, *345*, 672.

(19) Yu, F. H.; Yarov-Yarovoy, V.; Gutman, G. A.; Catterall, W. A. Overview of molecular relationships in the voltage-gated ion channel superfamily. *Pharmacol. Rev.* **2005**, *57*, 387−395.

(20) Bustamante, C.; Marko, J. F.; Siggia, E. D.; Smith, S. Entropic elasticity of lambda-phage DNA. *Science* **1994**, *265*, 1599−600.

(21) Rief, M.; Gautel, M.; Oesterhelt, F.; Fernandez, J. M.; Gaub, H. E. Reversible unfolding of individual titin immunoglobulin domains by AFM. *Science* **1997**, *276*, 1109−1112.

(22) Peng, Q.; Li, H. Atomic force microscopy reveals parallel mechanical unfolding pathways of T4 lysozyme: evidence for a kinetic partitioning mechanism. *Proc. Natl. Acad. Sci. U.S.A.* **2008**, *105*, 1885−1890.

(23) Kotamarthi, H. C.; Sharma, R.; Narayan, S.; Ray, S.; Ainavarapu, S. R. Multiple unfolding pathways of leucine binding protein (LBP) probed by single-molecule force spectroscopy (SMFS). *J. Am. Chem. Soc.* **2013**, *135*, 14768−14774.

(24) Maity, S.; Mazzolini, M.; Arcangeletti, M.; Valbuena, A.; Fabris, P.; Lazzarino, M.; Torre, V. Conformational rearrangements in the transmembrane domain of CNGA1 channels revealed by single-molecule force spectroscopy. *Nat. Commun.* **2015**, *6*, No. 7093.

(25) Marchesi, A.; Mazzolini, M.; Torre, V. Gating of cyclic nucleotide-gated channels is voltage dependent. *Nat. Commun.* **2012**, *3*, No. 973.

(26) Gorostiza, P.; Tombola, F.; Verdaguer, A.; Smith, S. B.; Bustamante, C.; Isacoff, E. Y. Molecular handles for the mechanical manipulation of single-membrane proteins in living cells. *IEEE Trans. Nanobiosci.* **2005**, *4*, 269−276.

(27) Santacroce, M.; Daniele, F.; Cremona, A.; Scaccabarozzi, D.; Castagna, M.; Orsini, F. Imaging of *Xenopus laevis* oocyte plasma membrane in physiological-like conditions by atomic force microscopy. *Microsc. Microanal.* **2013**, *19*, 1358−1363.

(28) Kaupp, U. B.; Niidome, T.; Tanabe, T.; Terada, S.; Bönigk, W.; Stühmer, W.; Cook, N. J.; Kangawa, K.; Matsuo, H.; Hirose, T. Primary structure and functional expression from complementary DNA of the rod photoreceptor cyclic GMP-gated channel. *Nature* **1989**, *342*, 762−766.

(29) Anderson, P. A.; Greenberg, R. M. Phylogeny of ion channels: clues to structure and function. *Comp. Biochem. Physiol., Part B: Biochem. Mol. Biol.* **2001**, *129*, 17−28.

(30) Kaupp, U. B.; Seifert, R. Cyclic nucleotide-gated ion channels. *Physiol. Rev.* **2002**, *82*, 769−824.

(31) Matulef, K.; Zagotta, W. N. Multimerization of the ligand binding domains of cyclic nucleotide-gated channels. *Neuron* **2002**, *36*, 93−103.

(32) Nair, A. V.; Anselmi, C.; Mazzolini, M. Movements of native C505 during channel gating in CNGA1 channels. *Eur. Biophys. J.* **2009**, *38*, 465−478.

(33) Mazzolini, M.; Punta, M.; Torre, V. Movement of the C-helix during the gating of cyclic nucleotide-gated channels. *Biophys. J.* **2002**, *83*, 3283−3295.

(34) Craven, K. B.; Zagotta, W. N. CNG and HCN channels: two peas, one pod. *Annu. Rev. Physiol.* **2006**, *68*, 375−401.

(35) Mazzolini, M.; Marchesi, A.; Giorgetti, A.; Torre, V. Gating in CNGA1 channels. *Pfluegers Arch.* **2010**, *459*, 547−555.

(36) Higgins, M. K.; Weitz, D.; Warne, T.; Schertler, G. F.; Kaupp, U. B. Molecular architecture of a retinal cGMP-gated channel: the arrangement of the C domains. *EMBO J.* **2002**, *21*, 2087−2094.

(37) Zagotta, W. N.; Olivier, N. B.; Black, K. D.; Young, E. C.; Olson, R.; Gouaux, E. Structural basis for modulation and agonist specificity of HCN pacemaker channels. *Nature* **2003**, *425*, 200−205.

(38) Schünke, S.; Stoldt, M.; Lecher, J.; Kaupp, U. B.; Willbold, D. Structural insights into conformational changes of a cyclic nucleotide-binding domain in solution from Mesorhizobium loti K1 channel. *Proc. Natl. Acad. Sci. U.S.A.* **2011**, *108*, 6121−6126.

(39) Lolicato, M.; Nardini, M.; Gazzarrini, S.; Möller, S.; Bertinetti, D.; Herberg, F. W.; Bolognesi, M.; Martin, H.; Fasolini, M.; Bertrand, J. A.; Arrigoni, C. Tetramerization dynamics of C-terminal domain underlies isoform-specific cAMP gating in hyperpolarization-activated cyclic nucleotide-gated channels. *J. Biol. Chem.* **2011**, *286*, 44811−44820.

(40) Derebe, M. G.; Zeng, W.; Li, Y.; Alam, A.; Jiang, Y. Structural studies of ion permeation and Ca2+ blockage of a bacterial channel mimicking the cyclic nucleotide-gated channel pore. *Proc. Natl. Acad. Sci. U.S.A.* **2011**, *108*, 592−597.

DOI: 10.1021/acsomega.6b00202
ACS Omega 2016, 1, 1205−1219

(41) Napolitano, L. M.; Bisha, I.; De March, M.; Marchesi, A.; Arcangeletti, M.; Demitri, N.; Mazzolini, M.; Rodriguez, A.; Magistrato, A.; Onesti, S.; Laio, A. A structural, functional, and computational analysis suggests pore flexibility as the base for the poor selectivity of CNG channels. *Proc. Natl. Acad. Sci. U.S.A.* **2015**, *112*, E3619−E3628.
(42) Bénitah, J. P.; Tomaselli, G. F.; Marban, E. Adjacent pore-lining residues within sodium channels identified by paired cysteine mutagenesis. *Proc. Natl. Acad. Sci. U.S.A.* **1996**, *93*, 7392−7396.
(43) Holmgren, M.; Shin, K. S.; Yellen, G. The activation gate of a voltage-gated K+ channel can be trapped in the open state by an intersubunit metal bridge. *Neuron* **1998**, *21*, 617−621.
(44) Glusker, J. P. Structural aspects of metal liganding to functional groups in proteins. *Adv. Protein Chem.* **1991**, *42*, 1−76.
(45) Hastrup, H.; Karlin, A.; Javitch, J. A. Symmetrical dimer of the human dopamine transporter revealed by cross-linking Cys-306 at the extracellular end of the sixth transmembrane segment. *Proc. Natl. Acad. Sci. U.S.A.* **2001**, *98*, 10055−10060.
(46) Akabas, M. H.; Stauffer, D. A.; Xu, M.; Karlin, A. Acetylcholine receptor channel structure probed in cysteine-substitution mutants. *Science* **1992**, *258*, 307−310.
(47) Karlin, A.; Akabas, M. H. Substituted-cysteine accessibility method. *Methods Enzymol.* **1998**, *293*, 123−145.
(48) Becchetti, A.; Roncaglia, P. Cyclic nucleotide-gated channels: intra- and extracellular accessibility to Cd2+ of substituted cysteine residues within the P-loop. *Pfluegers Arch.* **2000**, *440*, 556−565.
(49) Jiang, Y.; Lee, A.; Chen, J.; Cadene, M.; Chait, B. T.; MacKinnon, R. The open pore conformation of potassium channels. *Nature* **2002**, *417*, 523−526.
(50) Jiang, Y.; Lee, A.; Chen, J.; Ruta, V.; Cadene, M.; Chait, B. T.; MacKinnon, R. X-ray structure of a voltage-dependent K+ channel. *Nature* **2003**, *423*, 33−41.
(51) Nair, A. V.; Nguyen, C. H.; Mazzolini, M. Conformational rearrangements in the S6 domain and C-linker during gating in CNGA1 channels. *Eur. Biophys. J.* **2009**, *38*, 993−1002.
(52) Mazzolini, M.; Anselmi, C.; Torre, V. The analysis of desensitizing CNGA1 channels reveals molecular interactions essential for normal gating. *J. Gen. Physiol.* **2009**, *133*, 375−386.
(53) Nair, A. V.; Anselmi, C.; Mazzolini, M. Movements of native C505 during channel gating in CNGA1 channels. *Eur. Biophys. J.* **2009**, *38*, 465−478.
(54) Rosenbaum, T.; Gordon, S. E. Dissecting intersubunit contacts in cyclic nucleotide-gated ion channels. *Neuron* **2002**, *33*, 703−713.
(55) Mazzolini, M.; Nair, A.; Torre, V. A comparison of electrophysiological properties of the CNGA1, CNGA1tandem and CNGA1cys-free Channels. *Eur. Biophys. J.* **2008**, *37*, 947−959.
(56) Park, P. S.; Müller, D. J. Dynamic single-molecule force spectroscopy of rhodopsin in native membranes. *Methods Mol. Biol.* **2015**, *1271*, 173−185.
(57) Bell, G. I. Models for the specific adhesion of cells to cells. *Science* **1978**, *200*, 618−627.
(58) Evans, E.; Ritchie, K. Dynamic strength of molecular adhesion bonds. *Biophys. J.* **1997**, *72*, 1541−1555.
(59) Macdonald, B.; McCarley, S.; Noeen, S.; van Giessen, A. E. Protein-protein interactions affect alpha helix stability in crowded environments. *J. Phys. Chem. B* **2015**, *119*, 2956−2967.
(60) Arinaminpathy, Y.; Sansom, M. S.; Biggin, P. C. Molecular dynamics simulations of the ligand-binding domain of the ionotropic glutamate receptor GluR2. *Biophys. J.* **2002**, *82*, 676−683.
(61) Yarov-Yarovoy, V.; DeCaen, P. G.; Westenbroek, R. E.; Pan, C. Y.; Scheuer, T.; Baker, D.; Catterall, W. A. Structural basis for gating charge movement in the voltage sensor of a sodium channel. *Proc. Natl. Acad. Sci. U.S.A.* **2012**, *109*, E93−E102.
(62) Domene, C.; Sansom, M. S. Potassium channel, ions, and water: simulation studies based on the high resolution X-ray structure of KcsA. *Biophys. J.* **2003**, *85*, 2787−2800.
(63) Arcangeletti, M.; Marchesi, A.; Mazzolini, M.; Torre, V. Multiple mechanisms underlying rectification in retinal cyclic nucleotide-gated (CNGA1) channels. *Physiol. Rep.* **2013**, *1*, No. E00148.
(64) Laio, A.; Torre, V. Physical origin of selectivity in ionic channels of biological membranes. *Biophys. J.* **1999**, *76*, 129−148.

DOI: 10.1021/acsomega.6b00202
ACS Omega 2016, 1, 1205−1219